Cellular and Molecular Life Sciences (2025) 82:39
https://doi.org/10.1007/s00018-024-05558-9

ORIGINAL ARTICLE

The protective effects of liraglutide in reducing lipid droplets accumulation and myocardial fibrosis in diabetic cardiomyopathy

Chien-Yin Kuo[1,2] · Sing-Hua Tsou[3] · Edy Kornelius[4,5] · Kuei-Chuan Chan[4,5] · Kai-Wei Chang[4] · Jung-Chi Li[6] · Chien-Ning Huang[1,4] · Chih-Li Lin[1,3]

Received: 25 August 2024 / Revised: 8 November 2024 / Accepted: 18 December 2024

Abstract

Background Diabetes is a primary contributor to diabetic cardiomyopathy (DbCM), which is marked by metabolic imbalances such as elevated blood glucose and lipid levels, leading to significant structural and functional alterations in the myocardium. Elevated free fatty acids (FFAs) and hyperglycemia play critical roles in DbCM development, with FFAs inducing insulin resistance in cardiomyocytes and promoting lipid accumulation, resulting in oxidative stress and fibrosis. Current research suggests that glucagon-like peptide-1 (GLP-1) receptor agonists may effectively mitigate DbCM, although an effective treatment for this condition remains elusive, and the precise mechanisms of this protective effect are not fully understood.

Methods In this study, we aimed to replicate diabetic glucolipotoxic conditions by treating differentiated H9c2 cells with high glucose and free fatty acids. Additionally, a diabetic cardiomyopathy model was induced in mice through high-fat diets. Both in vitro and in vivo models were used to investigate the protective effects of liraglutide on cardiomyocytes and elucidate its underlying molecular mechanisms.

Results Our findings indicate that liraglutide significantly reduces lipid droplet (LD) formation and myocardial fibrosis, as evidenced by decreased expression of fibrosis markers, including TGF-β1 and collagen types I and III. Liraglutide also enhanced AMP-activated protein kinase (AMPK) activation, which improved mitochondrial function, increased antioxidant gene expression, enhanced insulin signaling, and reduced oxidative stress.

Conclusions These results demonstrate the potential therapeutic role of liraglutide in managing diabetes-related cardiac complications, offering a comprehensive approach to improving cardiac outcomes in patients with diabetes.

Chien-Yin Kuo, Sing-Hua Tsou and Edy Kornelius authors contributed equally to this work.

Extended author information available on the last page of the article

Published online: 08 January 2025

Graphical abstract

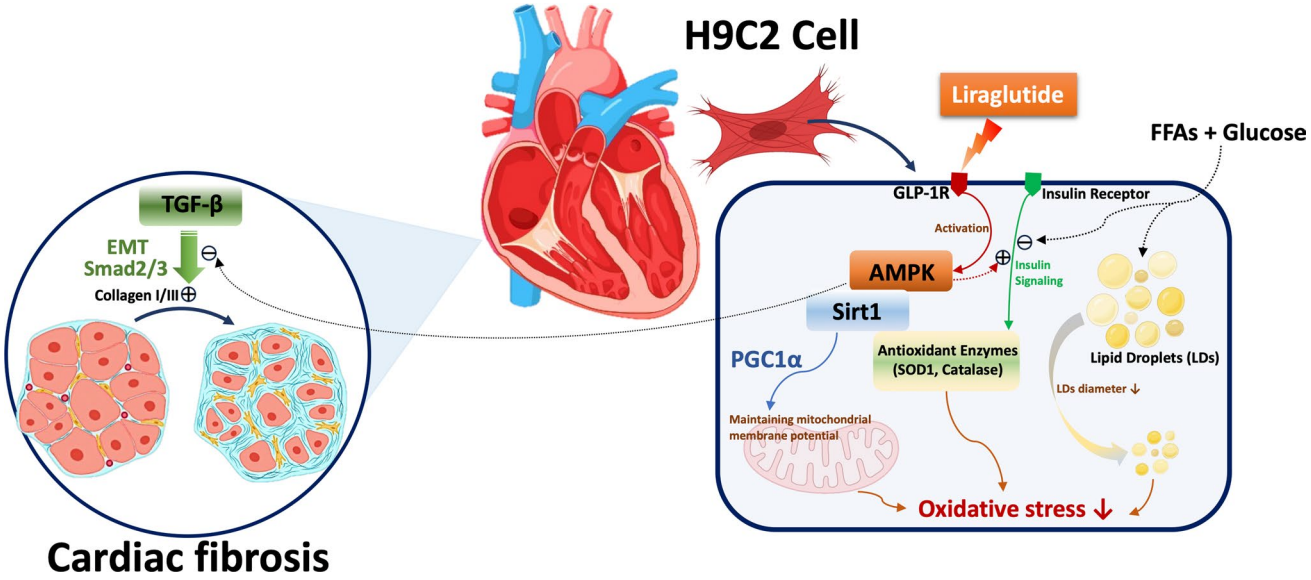

Keywords Diabetic cardiomyopathy · Liraglutide · Lipid droplet · Fibrosis · AMP-activated protein kinase (AMPK)

Introduction

Diabetes is the primary cause of diabetic cardiomyopathy (DbCM), a cardiac disorder characterized by metabolic imbalances, including elevated blood glucose and lipid levels, which substantially alter myocardial structure and function. DbCM is associated with a heightened risk of progression to overt heart failure, with most patients exhibiting preserved left ventricular ejection fraction (LVEF) [1]. This condition significantly elevates the morbidity and mortality rates in heart failure (HF) [2]. Notably, patients with type 2 diabetes (T2D) have up to a 74% increased risk of HF, and diabetic patients who develop HF experience a four-fold increase in mortality compared to those without HF [3]. However, treating DbCM in the context of T2D presents challenges due to the complex interaction of metabolic and cardiovascular factors. Hyperglycemia and elevated free fatty acids (FFAs) are primary drivers of DbCM development [4]. Lipotoxicity, exacerbated by elevated FFAs, contributes to cardiac dysfunction by disrupting glucose uptake and inducing insulin resistance in cardiomyocytes [5]. This insulin resistance further promotes lipid accumulation within cardiac cells, leading to oxidative stress [6]. The resulting imbalance between reactive oxygen species (ROS) production and antioxidant defenses promotes oxidative stress, fostering fibrosis and cellular injury [7]. Additionally, FFA-induced lipotoxicity impairs mitochondrial function, crucial for cardiomyocyte energy production [8]. Mitochondrial dysfunction results in decreased ATP production and increased ROS generation, compounding cellular stress and damage [9]. Understanding these molecular pathways is essential for developing targeted therapies aimed at slowing or preventing the progression of DbCM. Further studies focusing on these mechanisms could inform novel therapeutic approaches to improve outcomes for patients with this debilitating condition.

Intracellular lipid accumulation induced by glucolipotoxicity is a key factor in the progression of DbCM [10]. Elevated glucose and FFA levels promote the formation of lipid droplets (LDs) within cardiomyocytes, disrupting normal cellular metabolic processes and increasing oxidative stress [11]. This condition also activates transforming growth factor β (TGF-β)-related signaling pathways [12]. Particularly, it plays a significant role by upregulating the expression of profibrotic genes via the Smad pathway [13]. Upon receptor binding, TGF-β phosphorylates Smad2 and Smad3, which then form a complex with Smad4. This complex translocates to the nucleus, promoting the transcription of fibrotic genes, including those encoding collagen I, collagen III, and α-smooth muscle actin (αSMA) [11]. Collagen I and III are major components of the extracellular matrix (ECM) in fibrotic tissue, contributing to myocardial stiffness and impaired cardiac function [14]. In summary, LD accumulation induces oxidative stress, which in turn activates

TGF-β signaling, leading to fibrosis in DbCM [15]. While specific inhibitors exist to target these individual mechanisms, their single-target approach often results in limited efficacy and increased side effects [16]. Developing multifaceted therapeutic strategies that concurrently address these interconnected pathways may prove more effective in reducing DbCM progression, particularly fibrosis. Such a comprehensive approach could prevent LD accumulation, inhibit fibrotic gene expression, and mitigate pathological cardiac remodeling, thereby improving cardiac function and patient outcomes [17].

Recent research has shown that sodium-glucose cotransporter-2 (SGLT2) inhibitors, initially developed as antidiabetic agents, may also provide significant benefits in preventing heart failure [18]. Consequently, these drugs have been incorporated into heart failure treatment guidelines. Despite the minimal expression of SGLT2 in myocardial tissue, SGLT2 inhibitors appear to improve cardiac outcomes through various mechanisms unrelated to glucose excretion [19]. A primary mechanism involves their diuretic effect, which reduces fluid and sodium retention, thereby lowering cardiac workload. This effect is particularly beneficial for patients with heart failure, who often experience hypertension and fluid overload [20]. Additionally, SGLT2 inhibitors help lower blood glucose levels, thereby reducing inflammation and oxidative stress [21]. Notably, glucagon-like peptide-1 receptor agonists (GLP-1 RAs) have also garnered attention for their potential cardioprotective effects [22]. Unlike SGLT2 inhibitors, GLP-1 receptors (GLP-1R) are present in myocardial tissue, allowing GLP-1 RAs to exert direct effects on the heart [23]. These receptors mediate several cardioprotective actions, including reduced myocardial inflammation [24], smaller myocardial infarction size [25], and enhanced myocardial glucose oxidation [26]. Collectively, these mechanisms contribute to the cardioprotective effects observed with GLP-1 RAs, positioning them as a promising treatment option for patients with both diabetes and heart failure. However, despite considerable evidence supporting the cardioprotective effects of GLP-1 RAs, gaps remain in understanding their precise molecular mechanisms in DbCM. This study aims to elucidate the effects and molecular pathways of the GLP-1 RA liraglutide on myocardial cells under hyperglycemic and hyperlipidemic conditions typical of diabetes. Special focus is placed on the influence of liraglutide on lipid droplet accumulation and fibrosis in myocardial cells. By exploring these aspects, this investigation seeks to deepen the understanding of how liraglutide can mitigate cardiac complications in diabetic patients and enhance therapeutic strategies for DbCM.

Materials and Methods

Materials

Sigma-Aldrich (Munich, Germany) supplied the chemicals used in this study, including 3-(4,5-dimethylthiazol-2-yl)-2,5-diphenyltetrazolium bromide (MTT), 4′,6-diamidino-2-phenylindole (DAPI), 2′,7′-dichlorodihydrofluorescein diacetate (DCFH-DA), LY24002, compound C, JC-1, and Nile red. Antibodies were sourced from several suppliers: Santa Cruz Biotechnology (Santa Cruz, CA, USA) provided PGC1α (sc-517380; RRID:AB_2755043), Akt (sc-5298; RRID:AB_626658), phospho-Akt (sc-514032; RRID:AB_2861344), Talin 1 (sc-81805; RRID:AB_2303406), Integrin β1 (sc-374429; RRID:AB_11012020), and TGF-β1 (sc-130348; RRID:AB_1567351). GeneTex (Irvine, CA, USA) supplied antibodies for vimentin (GTX100619; RRID:AB_1952557), SOD1 (GTX100659; RRID:AB_1951972), catalase (GTX110704; RRID:AB_1949848), and Sirt1 (GTX61042; RRID:AB_10619663). ABclonal (Woburn, MA, USA) provided antibodies for GLP-1R (A13990; RRID:AB_2760844), αSMA (A2235; RRID:AB_2862980), and E-cadherin (A20798; RRID:AB_3107194), while Cell Signaling Technology (Danvers, MA, USA) supplied AMPK (#2532; RRID:AB_330331), phospho-AMPK (#2531; RRID:AB_330330), Smad2/3 (#5678; RRID:AB_10693547), and phospho-Smad2/3 (#8828; RRID:AB_2631089). Antibodies for IRS1 (05–1085; RRID:AB_1977296) and phospho-IRS1 (05–1087; RRID:AB_1977300) were obtained from Millipore (Bedford, MA, USA), and β-actin (NB600-501; RRID:AB_10077656) from Novus Biologicals (Littleton, CO, USA). Collagen I (ARG21965) and Collagen III (ARG20786) were acquired from Arigo Biolaboratories (Burlington, NC, USA), and liraglutide was sourced from Novo Nordisk (Copenhagen, Denmark). All chemicals were dissolved in phosphate-buffered saline (PBS) and stored at -20 °C until required for experimentation.

Cell culture and differentiation

Rat H9c2 cardiac myoblast cells (RRID:CVCL_0286) were obtained from the American Type Culture Collection (Bethesda, MD, USA). Cells were cultured in 75 cm^2 tissue culture flasks using DMEM medium supplemented with 10% fetal bovine serum (FBS) and 1% penicillin–streptomycin. Cultures were maintained at 37 °C with 5% CO_2 in a humidified atmosphere. To preserve differentiation potential, the supplier recommended subculturing the cells before reaching 70–80% confluence. When the cells reached approximately 50–60% confluence, the culture medium was

replaced with differentiation medium. This differentiation medium, consisting of DMEM with 1% FBS and 10 nM all-trans retinoic acid (ATRA), was refreshed every 2–3 days, and the cells were maintained in this medium for 11 days. Differentiation was confirmed by observing morphological changes under a microscope, including cell elongation and alignment.

Immunocytochemistry

After treatment, ells were rinsed with PBS up to three times following removal of the culture medium. Cells were then fixed by adding 4% paraformaldehyde (PFA) in PBS to each well and incubated for 15–20 min at room temperature. Residual PFA was removed by washing the cells three times with PBS. To permeabilize, cells were incubated with 0.1% Triton X-100 in PBS at room temperature for 10 min. After three PBS washes, non-specific binding sites were blocked by incubating cells overnight at 4 °C in a humidified chamber with a blocking solution. Cells were then incubated in a humidified chamber at 4 °C overnight with the primary antibody diluted 1:100. Afterward, cells were incubated with the secondary antibody, diluted 1:200, in the dark at room temperature for 1 h. Stained cells were examined using the ImageXpress Micro Confocal High-Content Imaging System (Molecular Devices, Sunnyvale, CA, USA).

Nile red staining and high-content analysis (HCA)

Following treatment, cells were fixed with 4% paraformaldehyde for 15 min, then rinsed with PBS. Nile red staining (1 μg/mL) was performed in the dark at room temperature for five minutes. Imaging was carried out using the ImageXpress Micro Confocal High-Content Imaging System (Molecular Devices, Sunnyvale, CA, USA). Quantitative analysis of Nile red-stained particles was automated with a custom module in MetaXpress software (Molecular Devices, Sunnyvale, CA, USA), examining a minimum of 100 cells per well, with each condition performed in triplicate.

mRNA expression analysis by reverse-transcription quantitative PCR (qPCR)

Total RNA was isolated from cultured cells using Trizol reagent (Invitrogen, USA) according to the manufacturer's instructions. After extraction, RNA purity and concentration were assessed by measuring absorbance at 260/280 nm with a spectrophotometer. The RNA was then reverse-transcribed into complementary DNA (cDNA) using a high-capacity cDNA reverse transcription kit (Thermo Fisher Scientific, Waltham, MA, USA). Quantitative real-time PCR was performed using a Roche LightCycler 480 Real-Time PCR system (Roche, Basel, Switzerland) with SYBR Green PCR Master Mix (Roche, Basel, Switzerland) for mRNA detection. Reactions were conducted in a 20 μL volume containing 10 μL of SYBR Green Master Mix, 1 μL of each primer (10 μM), 2 μL of cDNA template, and 6 μL of nuclease-free water. GAPDH was used as the internal control for normalization. The thermal cycling conditions were set as follows: an initial denaturation at 95 °C for 10 min, followed by 40 cycles of 95 °C for 15 s, 60 °C for 30 s, and 72 °C for 30 s. Primer sequences are provided in Table 1. Melt curve analysis was conducted at the end of each run to confirm specificity of the amplification. Relative expression levels were calculated using the $2^{-\Delta\Delta CT}$ method, normalizing to GAPDH

Table 1 Primer sequence of different genes for qPCR analysis

Genes	Forward (5′-3′)	Reverse (5′-3′)
COL1A1 (Collagen Type I α1 Chain)	GGATCGACCCTAACCAAGGC	GATCGGAACCTTCGCTICCA
COL3A1 (Collagen Type III α1 Chain)	GGTCACTITCACTGGTTGACGA	TTGAATATCAAACACGCAAGGC
TGFB1 (Transforming Growth Factor β1)	ACTACTACGCCAAGGAGGTCAC	AGAGCAACACGGGTTCAGGTA
GDNF (Glial Cell-Derived Neurotrophic Factor)	CTCGAAGTAGAAGGCTAACA	AGCGGAATGCTTTCTTAGG
NGF (Nerve Growth Factor)	ACCTCTTCGGACACTCTGG	CGTGGCTGTGGTCTTATCTC
BDNF (Brain-Derived Neurotrophic Factor)	CGAGACCAAGTGTAATCCCA	TCTATCCTTATGAACCGCCA
FABP3 (Fatty Acid Binding Protein 3)	ACACTTGTGCGGGAGCTAAT	CATGGGAACTGGAACTGGAT
GAPDH (Glyceraldehyde-3-Phosphate Dehydrogenase)	GAGCGAGATCCCGTCAAGATCAAA	CACAGTCTTCTGAGTGGCAGTGAT

and comparing to control samples. All samples were run in triplicate to ensure data reliability, and negative controls (no-template controls) were included to rule out contamination.

Western blot analysis

Cells were washed twice with cold PBS and lysed using Gold lysis buffer (10 mM Tris–HCl, pH 7.4, 150 mM NaCl, 1% Triton X-100, 1 mM EDTA, 1 mM EGTA, 0.5% sodium deoxycholate, 0.1% SDS, and protease/phosphatase inhibitors). For animal tissue samples, tissue was homogenized in T-PER Tissue Protein Extraction Reagent (Thermo Fisher Scientific, Waltham, MA, USA) at a ratio of 1:20 (w/v), tissue to T-PER reagent, to ensure efficient extraction. The homogenate was then centrifuged at 12,000 × g for 15 min at 4 °C to pellet cell or tissue debris. The supernatant containing the total protein extract was collected, and protein concentration was determined using a BCA protein assay kit (BioRad, Hercules, CA, USA), following the manufacturer's protocol. Equal amounts of protein (20–40 µg) from each sample were loaded into each well of an SDS-PAGE gel. Following electrophoresis, proteins were transferred to a PVDF membrane using a wet transfer apparatus. Membranes were blocked with blocking buffer and then incubated with primary antibodies (1:1000) at 4 °C overnight with gentle agitation. After washing, membranes were incubated with secondary antibodies (1:5000) for 1 h at room temperature with gentle agitation. Signal detection was performed using Amersham ECL detection kits (Cytiva, Marlborough, MA, USA), and signals were visualized using an AI600 imaging system (GE Healthcare, Chicago, IL, USA). Western blot band quantification was conducted using Image-Pro Plus 6.0 software (Media Cybernetics, Rockville, MD, USA).

Measurement of reactive oxygen species (ROS)

Following treatment, cells were incubated with DCFH-DA (10 µM) for 30 min to allow ROS-dependent conversion of DCFH-DA to the fluorescent DCF. Cells were then washed and resuspended in PBS. Fluorescence intensity, indicative of ROS levels, was measured using the SpectraMax iD5 multi-mode microplate reader (Molecular Devices, Sunnyvale, CA, USA) with excitation at 485 nm and emission at 535 nm. For normalization, ROS levels in treated samples were quantified as a percentage relative to the untreated control. This was achieved by calculating the fluorescence intensity ratio between treated samples and controls. Specifically, untreated control samples were measured to establish baseline ROS fluorescence, and ROS levels in treated samples were calculated using the formula:

$$\text{Relative ROS Level}(\%) = \frac{\text{Fluorescence Intensity of Treated Sample}}{\text{Fluorescence Intensity of Control Sample}} \times 100$$

Each treatment condition was assessed in triplicate to ensure reproducibility. This normalization allowed for direct comparison of ROS levels across different treatments, reported as a percentage of the control ROS level.

Lipid peroxidation measurement

Following treatment, cells were harvested by centrifugation at 3000 rpm for 10 min, and the supernatant was discarded. The cell pellets were resuspended in 300 µL of 10% medium and sonicated on ice for one minute. After adding 100 µL of precooled PBS, the cells were sonicated again and stored at -20 °C. Malondialdehyde (MDA) content, indicative of lipid peroxidation, was measured using the Lipid Peroxidation Assay Kit (BioVision, San Francisco, CA, USA) with colorimetric detection at 532 nm. Protein concentration was determined using a BCA protein assay kit (Millipore, Bedford, MA, USA), and MDA levels were normalized to protein content, expressed as nmol MDA per mg protein.

Mitochondrial membrane potential analysis

Mitochondrial functionality was evaluated using the cationic dye JC-1, which accumulates in mitochondria in a membrane potential-dependent manner. In healthy mitochondria, JC-1 forms red fluorescent aggregates, whereas in depolarized mitochondria under stress conditions, it remains as a monomer, emitting green fluorescence. After treatment, cells were incubated with 1 µM JC-1 at 37 °C for 30 min. Following incubation, the staining solution was removed, and cells were rinsed with PBS. Imaging was performed using an inverted fluorescence microscope (DP72/CKX41, Olympus, Tokyo, Japan). The red-to-green fluorescence ratio, indicative of mitochondrial membrane potential, was quantitatively analyzed using ImageJ software (National Institutes of Health, Bethesda, MD, USA).

Animal model preparation and experimental grouping

A schematic of the experimental design is shown in Fig. 5A. The study was conducted on 18 male db/db mice ($Lepr^{db/db}$, 5 weeks old) and 12 male wild-type (WT) mice (C57BL/6, 5 weeks old). All animals were housed in a specific pathogen-free (SPF) facility with controlled temperature (18–22 °C) and humidity (30–70%). Mice were given ad libitum access to water and food. After one week of acclimatization on a normal chow diet (5% fat by weight), mice were

randomly divided into five groups (n = 6) and assigned to the following dietary regimens for 24 weeks: normal chow, high-fat diet (HFD; 60% fat by weight, Envigo, Indianapolis, IN, USA), normal chow with C57BL/6 mice, HFD with C57BL/6 mice, normal chow with db/db mice, HFD with db/db mice, and HFD with db/db mice plus liraglutide. Body weight and fasting blood glucose levels (from tail vein samples) were recorded every four weeks. Liraglutide (0.4 mg/kg) was administered subcutaneously twice weekly to the designated groups for 24 weeks. At the study's conclusion, mice were anesthetized and euthanized to collect blood and tissue samples. Hearts were preserved in 4% buffered formalin for subsequent analysis. This study was approved by the Institutional Animal Care and Use Committee (IACUC) of Chung Shan Medical University (Approval No. 2673).

Histological examination and immunofluorescence staining

Following euthanasia, heart tissue was harvested and fixed in 4% neutral buffered formalin for 24 h. For cryosectional histological analysis, the heart was embedded in an optimal cutting temperature (OCT) compound and rapidly frozen using dry ice or liquid nitrogen. Sections were prepared at 16 µm thickness using a cryostat (CM3050S, Leica Biosystems, Nussloch, Germany) and collected onto pre-labeled, frost-free glass slides. Fibrosis in the heart was visualized by staining sections with Picrosirius red. Immunofluorescence staining was conducted by incubating sections with primary antibodies, followed by fluorescently labeled secondary antibodies. Nuclei were counterstained with DAPI in the mounting medium. Images were acquired using a fluorescence microscope (BX53, Olympus, Tokyo, Japan).

Statistical analysis

Data are presented as means ± standard error of the mean (SEM) and were analyzed using analysis of variance (ANOVA) followed by Dunnett's post-hoc test for multiple comparisons. Statistical analyses were performed using SPSS software (SPSS Inc., Chicago, IL, USA). A p-value of less than 0.05 was considered statistically significant.

Results

High glucose and FFAs induced the accumulation of lipid droplets (LDs) in differentiated H9c2 cells

Prior to experiments, H9c2 cardiomyoblasts were differentiated into cardiomyocytes following established protocols (Pereira, Ramalho-Santos et al. 2011). Once cells reached 70–80% confluence, serum concentration was reduced to 1%, and 10 nM all-trans retinoic acid (ATRA) was applied daily for eleven days (Fig. 1A). As shown in Fig. 1B, undifferentiated H9c2 cells displayed a short, spindle-shaped morphology, while differentiated cells adopted an elongated shape typical of cardiomyocytes. To model high glucose (HG) and high free fatty acid (HF) conditions similar to type 2 diabetes, differentiated cells were treated for 24 h with 250 µM FFAs (2:1 oleic acid to palmitic acid) and 55 mM glucose. These conditions did not significantly alter cell morphology or induce cell death, with similar outcomes noted upon co-treatment with 0.1 µM liraglutide. This suggests that the differentiated H9c2 cells tolerate glucolipotoxic conditions without acute toxicity. Next, we aimed to confirm GLP-1 receptor (GLP-1R) expression in differentiated H9c2 cells. Previous studies have demonstrated that cardiomyocytes exhibit significant GLP-1R expression [27]. To confirm GLP-1 receptor (GLP-1R) expression in differentiated H9c2 cells, immunocytochemistry was performed. As shown in Fig. 1C, GLP-1R expression was prominent in differentiated cells, and neither HG + HF conditions nor liraglutide treatment significantly impacted GLP-1R expression levels. Further analysis using Nile red staining revealed that HG + HF conditions led to notable lipid droplet (LD) accumulation within cardiomyocytes compared to controls, while co-treatment with liraglutide reduced this accumulation. Interestingly, under HG + HF conditions, GLP-1R and LDs showed notable co-localization, an effect reduced by liraglutide co-treatment. High-content analysis (HCA) revealed a significant increase in intracellular LDs in the HG + FFA group compared to controls, with approximately a threefold rise in LD count per cell. Liraglutide treatment reduced the LD count by 11% relative to the HG + FFA group, though it remained elevated at around 2.5 times the control levels. Further analysis of LD diameter showed that under HG + FFA conditions, there was a shift toward smaller LDs. Liraglutide treatment led to a 62% reduction in large LDs (> 0.5 µm) and an 8.7% increase in small LDs (< 0.5 µm) compared to the HG + FFA group. These results indicate that liraglutide, while having minimal impact on overall LD count, effectively inhibits the formation of larger LDs, suggesting a potential modulation of lipid storage under glucolipotoxic conditions (Fig. 1D).

Liraglutide attenuates the fibrosis caused by high glucose and FFAs in H9c2 cells

Excessive intracellular LD accumulation due to glucolipotoxicity is known to induce oxidative stress and inflammation, accelerating profibrotic pathway activation and leading to increased myocardial fibrosis. To evaluate liraglutide's effect on these processes, we measured the mRNA levels of fibrosis-related genes using qPCR, focusing on *TGFB1* (TGF-β1), *COL1A1* (collagen I), and

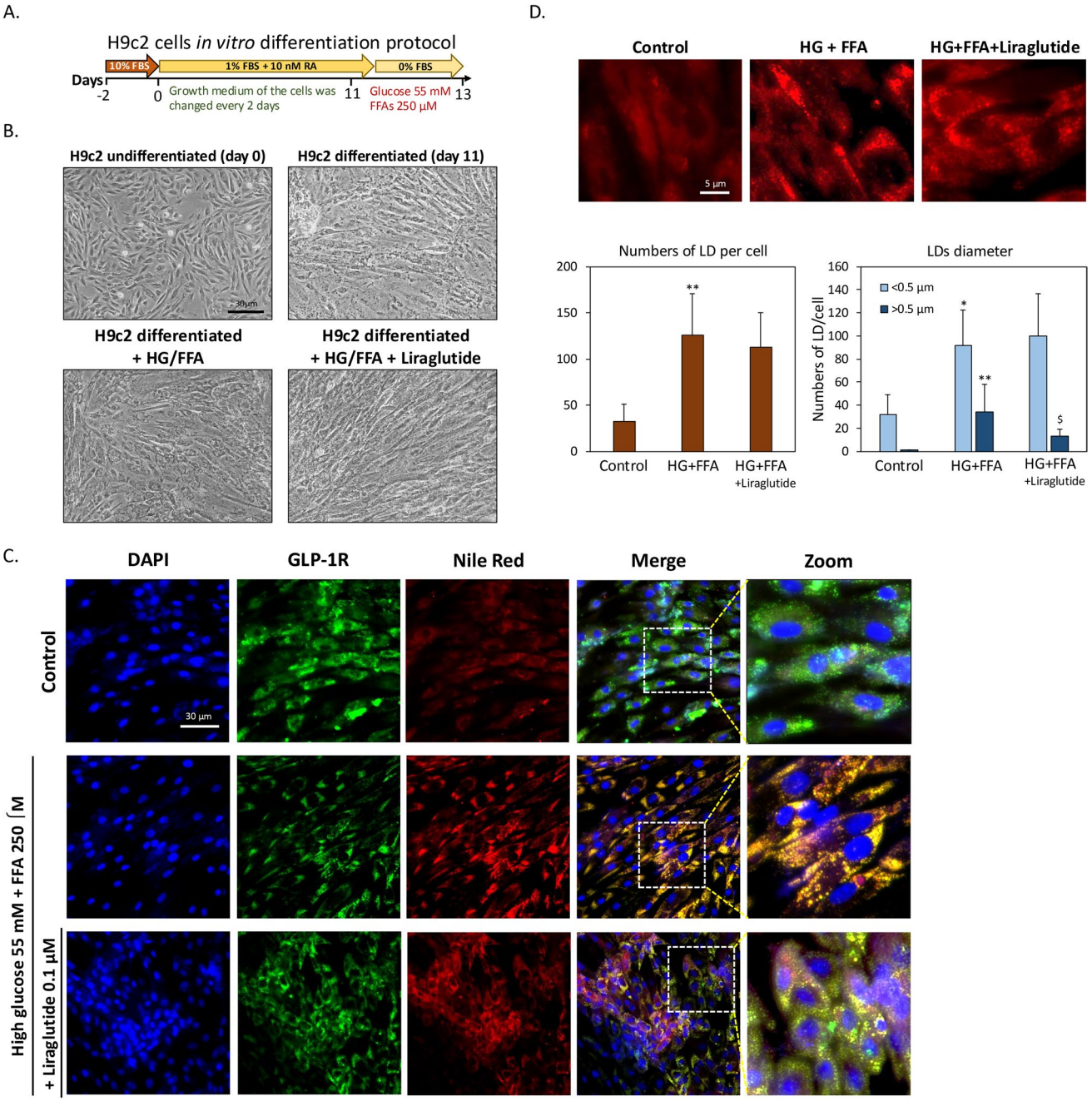

Fig. 1 Liraglutide prevents lipid droplet (LD) accumulation induced by high glucose (HG) and high free fatty acids (HF). **A** Protocol for differentiation of H9c2 cardiomyoblasts into cardiomyocytes. **B** Morphology of undifferentiated and differentiated H9c2 cells. The appearance of differentiated cells remained unchanged with the addition of HG + FFAs or liraglutide. **C** Immunofluorescence staining of GLP-1R (green) and LDs (red) in differentiated H9c2 cells. **D** High-content analysis (HCA) of LDs, showing the average number and size distribution of LDs per cell. Exposure to HG + HF for 24 h significantly increased LD count. Liraglutide did not significantly reduce the total LD count but decreased the number of larger LDs. (*$p < 0.05$ vs. control, **$p < 0.01$ vs. control, \$$p < 0.05$ vs. HG + FFA)

COL1A3 (collagen III). As shown in Fig. 2A, HG + HF conditions led to substantial increases in *TGFB1*, *COL1A1*, and *COL1A3* mRNA levels, reaching 546%, 265%, and 331% of control levels, respectively. Liraglutide treatment significantly mitigated these increases, reducing *TGFB1*, *COL1A1*, and *COL1A3* levels to 303%, 162%, and 159% of control levels, respectively. These results suggest that liraglutide effectively suppresses the expression of key fibrosis-related genes under HG + HF conditions, indicating a potential role in counteracting glucolipotoxicity-induced fibrosis. Western blot analysis, shown in Fig. 2B, further confirmed these findings. HG + HF conditions led to

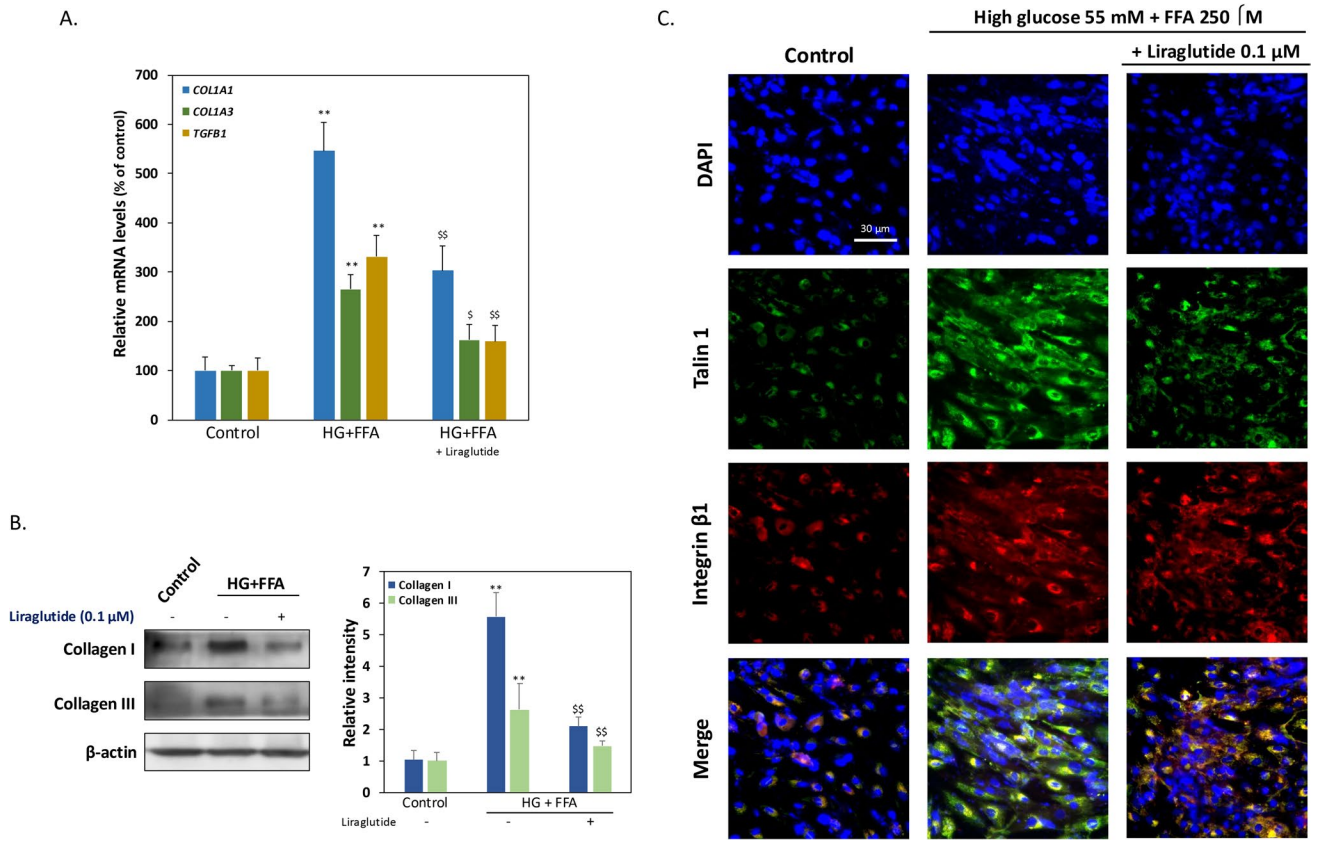

Fig. 2 Liraglutide inhibits fibrotic TGF-β and collagen synthesis induced by high glucose and FFAs. **A** Quantitative polymerase chain reaction (qPCR) analysis of fibrotic mRNA expression, including *COL1A1*, *COL1A3*, and *TGFB1*, in H9c2 cells. **B** Quantitative western blot analysis and representative blots for fibrotic markers collagen I and collagen III. **C** Immunofluorescence analysis of integrin β1 and its adapter protein talin 1. (**p < 0.01 vs. control, $p < 0.05 vs. HG + FFA, $$p < 0.01 vs. HG + FFA)

notable increases in collagen I and III protein expression, with collagen I at 460% and collagen III at 160% above control levels. Liraglutide treatment reduced these elevations, bringing collagen I to 210% and collagen III to 50% above control levels. This reinforces liraglutide's ability to inhibit HG + HF-induced protein expression of fibrosis-related markers. To explore the mechanism behind these effects, we examined integrin-related signaling, which is linked to TGF-β activation in diabetes [28]. Immunofluorescence staining of integrin β1 and talin 1 in H9c2 cells (Fig. 2C) revealed that HG + HF treatment markedly increased talin 1 expression, suggesting enhanced integrin-cytoskeletal linkage and signaling transmission. Liraglutide treatment reduced talin 1 expression significantly. A similar trend was observed for integrin β1, though liraglutide's inhibitory effect was less pronounced than for talin 1. In summary, HG + HF-induced LD accumulation promotes fibrosis-related collagen production in H9c2 cells, likely through integrin-mediated TGF-β activation. Liraglutide appears to counteract these effects, suggesting its potential to inhibit diabetic myocardial fibrosis by mitigating glucolipotoxicity's detrimental impact.

Liraglutide alleviates insulin signaling blockade and ROS accumulation induced by high glucose and FFAs

Metabolic disorders frequently result in insulin resistance, which contributes to cardiomyopathy in T2D and is exacerbated by oxidative stress, leading to cellular damage, fibrosis, and impaired cardiac function [29]. To assess liraglutide's protective effects under glucolipotoxic conditions, we analyzed insulin signaling, oxidative stress, mitochondrial function, and neurotrophic factor expression in H9c2 cells. As shown in Fig. 3A, HG + HF conditions increased $pSer^{307}$-IRS-1 protein expression by 30%, a marker of insulin resistance, and decreased $pSer^{473}$-Akt levels by 50%, indicating an insulin signaling blockade. Liraglutide treatment normalized these levels, reducing pSer307-IRS-1 back to control levels and restoring pSer473-Akt to 90%

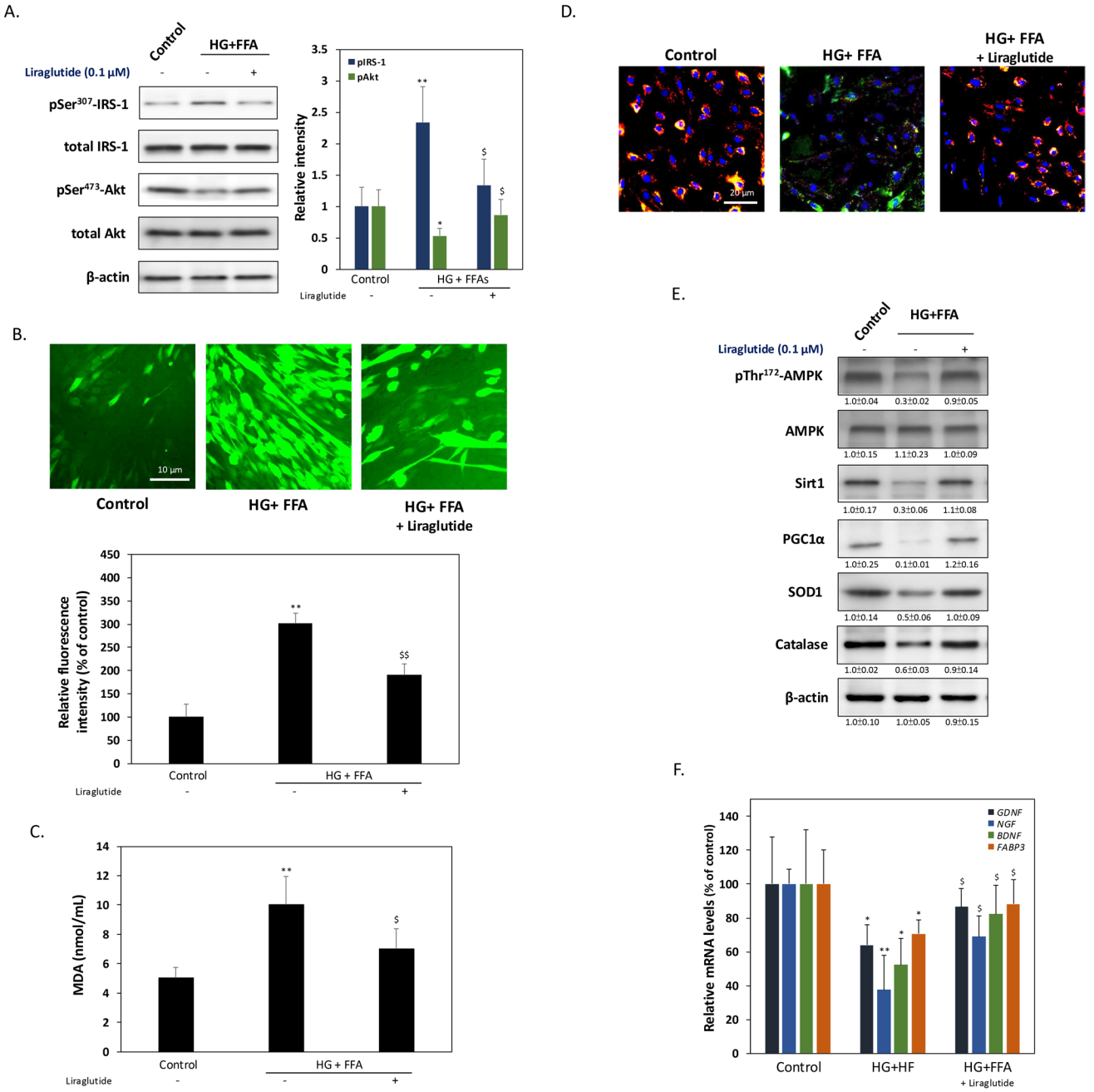

Fig. 3 Liraglutide attenuates insulin signaling blockade and ROS accumulation induced by high glucose and FFAs. **A** Western blot analysis showing changes in the protein expression of pSer^{307}-IRS-1 and pSer.^{473}-Akt, markers associated with insulin signaling. **B** DCFH-DA assay results demonstrating a significant increase in ROS levels after 24 h of HG + FFA exposure, which was markedly reduced by liraglutide treatment. **C** MDA content measurement to assess lipid peroxidation, showing an approximately 100% increase in MDA levels with HG + FFA treatment compared to control, indicating elevated oxidative stress. Liraglutide significantly reduced MDA levels, demonstrating its protective effect against oxidative damage. **D** Mitochondrial membrane potential was assessed using JC-1 staining, where healthy mitochondria are indicated by red fluorescence and dysfunctional mitochondria by green fluorescence. **E** Representative western blots and densitometric analysis for AMPK, Sirt1, PGC1α, SOD1, and catalase. **F** qPCR analysis of mRNA levels for neurotrophic factors *GDNF*, *NGF*, and *BDNF*, along with *FABP3*, a gene associated with nerve lipid metabolism. (*$p < 0.05$ vs. control, **$p < 0.01$ vs. control, \$$p < 0.05$ vs. HG + FFA, \$\$$p < 0.01$ vs. HG + FFA)

of control, suggesting reduced insulin resistance. ROS levels, assessed via DCFH-DA staining (Fig. 3B), showed a threefold increase under HG + HF conditions compared to controls, which liraglutide significantly inhibited, reducing ROS to 10% above control levels. In Fig. 3C, the results indicate that HG + FFA treatment significantly increased

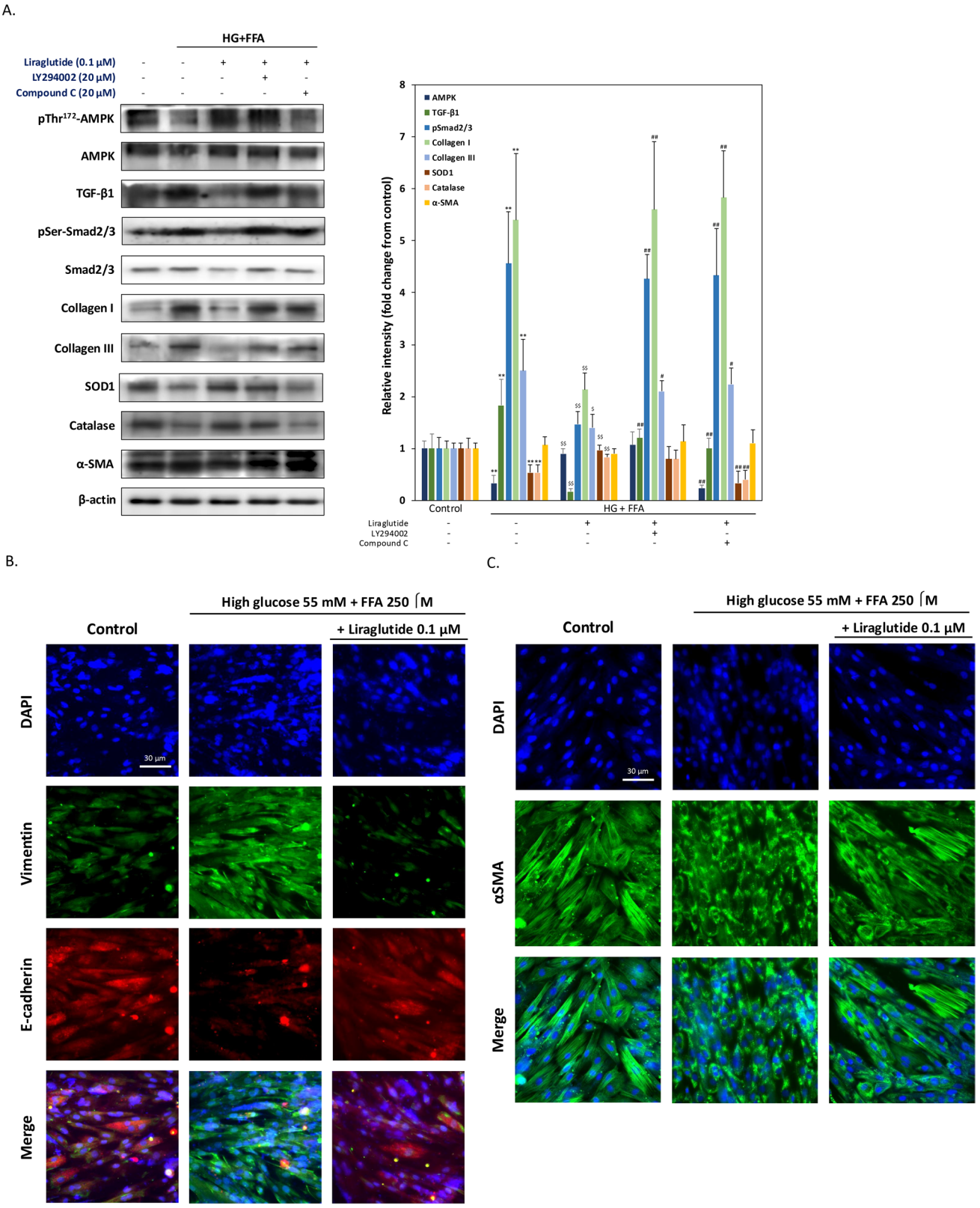

MDA content by approximately 100% compared to the control, demonstrating heightened oxidative stress. Liraglutide treatment effectively reduced MDA levels, indicating its protective role against oxidative damage. This finding aligns with the ROS results in Fig. 3B, further supporting liraglutide's antioxidative effects in mitigating cellular damage.

◂**Fig. 4** Liraglutide inhibits fibrosis by restoring insulin signaling, while AMPK activation reduces both oxidative stress and fibrosis. **A** Western blot analysis of the expression levels of p-AMPK, AMPK, TGF-β1, p-Smad2/3, Smad2/3, collagen I, collagen III, SOD1, catalase, and α-SMA. LY294002 was used as a PI3K inhibitor, and compound C (CC) as an AMPK inhibitor. **B** Immunofluorescence staining of EMT markers vimentin and E-cadherin, with DAPI used to stain nuclei. **C** Immunofluorescence analysis of α-SMA visualized by confocal microscopy. (**$p < 0.01$ vs. control, $p < 0.05$ vs. HG + FFA, $$p < 0.01$ vs. HG + FFA, #$p < 0.05$ vs. HG + FFA + Liraglutide, ##$p < 0.01$ vs. HG + FFA + Liraglutide)

Mitochondrial dysfunction, commonly observed under glucolipotoxicity, was evident in the JC-1 staining results (Fig. 3D), where HG + HF reduced mitochondrial membrane potential. However, co-treatment with liraglutide restored this potential, indicating its ROS-reducing effect may be partly due to improved mitochondrial function. Western blot analysis (Fig. 3E) revealed that HG + HF inhibited $pThr^{172}$-AMP-activated protein kinase (AMPK) and Sirt1, reduced PGC1α (critical for mitochondrial function), and decreased antioxidant genes like SOD1 and catalase, while liraglutide counteracted these effects, indicating its cell-protective role. Numerous studies have shown that nerve degeneration within myocardial tissue frequently occurs in diabetic cardiomyopathy, leading to compromised cardiac function [30]. To further investigate this phenomenon, we examined the expression of neurotrophic factors secreted by cardiomyocytes, including *GDNF* (glial cell line-derived neurotrophic factor), *NGF* (nerve growth factor), and *BDNF* (brain-derived neurotrophic factor), as shown in Fig. 3F. HG + HF significantly reduced the mRNA expression of neurotrophic factors *GDNF*, *NGF*, and *BDNF* by 36%, 62%, and 48%, respectively. Liraglutide partially restored these levels to 87%, 69%, and 82% of control, respectively, enhancing the conditions for nerve cell survival. Additionally, studies have shown that fatty acid binding protein 3 (FABP3) influences peripheral nerve survival in lipid metabolism disorders [31]. Our results showed that HG + HF decreased *FABP3* mRNA by 29%, while liraglutide treatment restored *FABP3* to 88% of control levels, suggesting a protective effect on peripheral nerves associated with metabolic disorders.

Liraglutide mitigates oxidative stress and fibrosis by restoring insulin signaling and enhancing AMPK

Liraglutide's mechanism of action is often associated with the AMPK and insulin signaling pathways [32]. To investigate this further, we used the selective inhibitors LY294002 (insulin signaling) and Compound C (AMPK) to assess liraglutide's protective effects in H9c2 cells under HG + HF conditions. As shown in Fig. 4A, HG + HF reduced $pThr^{173}$-AMPK expression by 70%, which liraglutide restored to 90% of control levels. The addition of Compound C decreased pAMPK by 80%, while LY294002 slightly increased pAMPK above control levels, indicating that liraglutide's activation of AMPK is independent of insulin signaling. HG + HF increased TGF-β1 expression by 80%, which liraglutide reduced by 80%. However, adding LY294002 or Compound C brought TGF-β1 levels up to 500% and 450% of control, respectively, suggesting liraglutide's effect on TGF-β1 involves both AMPK and insulin pathways. Similarly, HG + HF elevated pSmad2/3 levels by 360%, which liraglutide reduced by 70%; both inhibitors reversed this reduction, indicating liraglutide's suppression of pSmad2/3 requires both pathways. Collagen I and III levels increased by 440% and 150%, respectively, under HG + HF, but liraglutide reduced them by 60% and 44%. With LY294002 or Compound C, collagen I and III levels returned to those seen in HG + HF conditions, highlighting that liraglutide's antifibrotic effects depend on both AMPK and insulin signaling. For antioxidant enzymes, HG + HF decreased SOD1 and catalase levels by 50%. Liraglutide restored SOD1 to control levels and catalase to 80% of control. However, Compound C reduced both enzymes to 70% and 60% below control levels, indicating liraglutide's antioxidant effects are largely dependent on AMPK activation. This implies that liraglutide's modulation of insulin signaling primarily targets fibrosis, while its activation of AMPK influences both oxidative stress and fibrosis. TGF-β is also known to activate epithelial-mesenchymal transition (EMT), enhancing ECM protein secretion, altering tissue structure, and exacerbating fibrosis [33]. Immunofluorescence staining (Fig. 4B) showed that HG + HF increased the mesenchymal marker vimentin and decreased the epithelial marker E-cadherin in H9c2 cells. Liraglutide prevented this EMT shift, supporting its role in TGF-β signaling suppression. Lastly, while myocardial fibrosis has been linked to α-SMA, the immunoblotting results in Fig. 4A showed that α-SMA levels were not affected by HG + HF or liraglutide. However, immunofluorescence analysis (Fig. 4C) revealed that HG + HF disrupted α-SMA's long fiber structure, causing fragmentation and localized aggregates. Liraglutide restored α-SMA's distribution to a pattern comparable to the control group, further demonstrating its protective effect against glucolipotoxicity-induced cellular remodeling.

In vivo assessment of liraglutide's effect on myocardial fibrosis

Our in vitro studies indicated that liraglutide may inhibit diabetes-related myocardial fibrosis. To confirm our in vitro findings, we conducted in vivo animal experiments to strengthen the evidence for liraglutide's effects on diabetes-related myocardial fibrosis. As shown in Fig. 5A, wild-type (WT) and db/db mice were randomly assigned to receive either a normal chow or high-fat diet (HFD) at

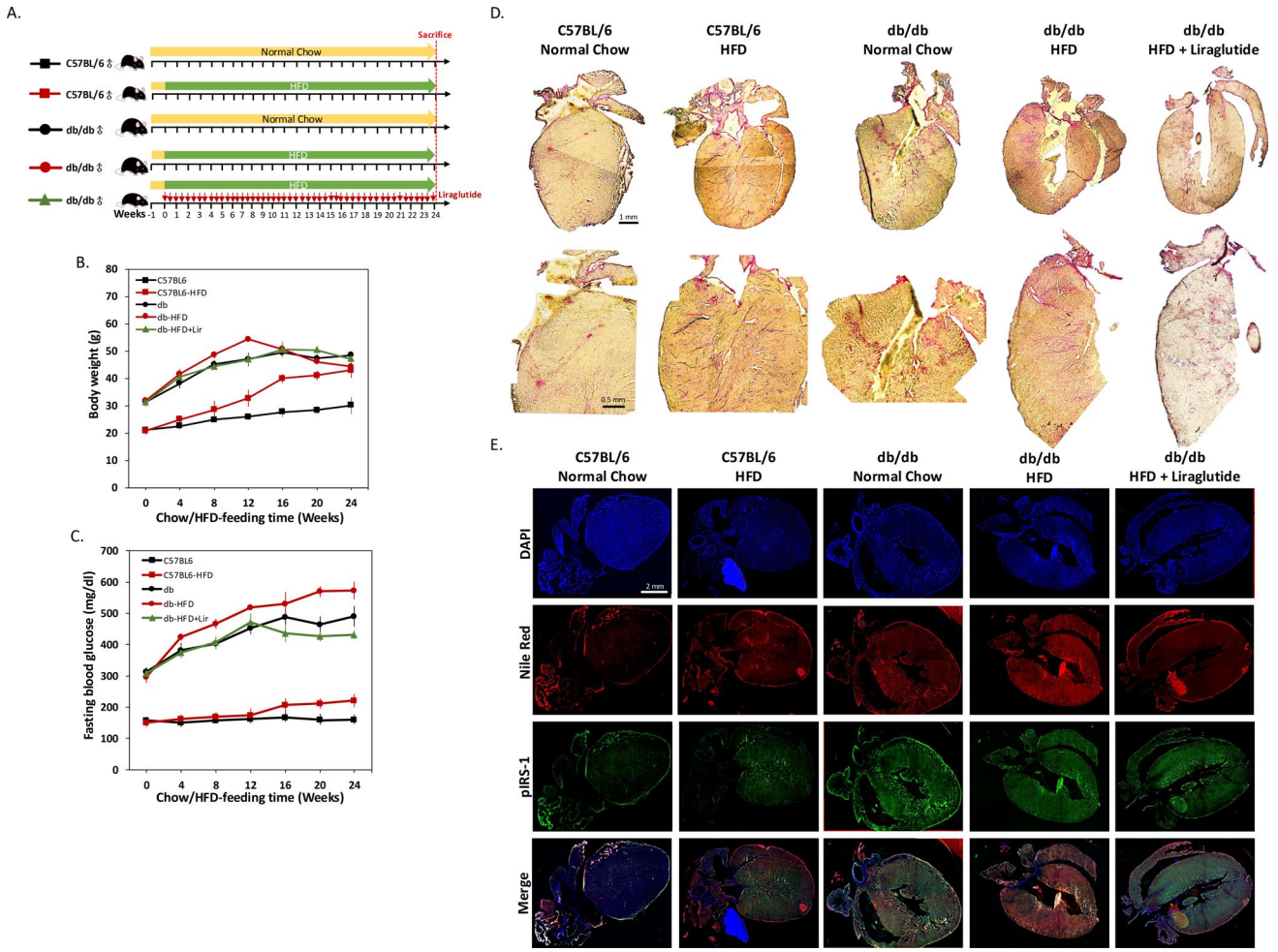

Fig. 5 Liraglutide reduces myocardial fibrosis and lipid accumulation in HFD-fed db/db mice. **A** Experimental protocol for animal treatment. Arrows indicate a single subcutaneous injection of liraglutide at 400 µg/kg. Animals were fed either an HFD or normal chow, as shown by the horizontal bars, with six animals per group. **B** Body weight measurements taken every four weeks. **C** Fasting blood glucose monitoring in animals fed normal chow, HFD, or HFD + liraglutide. **D** Representative images of cardiac sections stained with Picrosirius red staining, showing collagen deposition in red and various shades of yellow in cytoplasm and other protein-rich areas. **E** Immunofluorescence images of myocardial tissue stained with Nile red for lipid accumulation and pSer^{307}-IRS-1 to assess insulin resistance

6 weeks of age following a one-week acclimation period. A group of db/db mice on the HFD received subcutaneous liraglutide injections (400 µg/kg, twice weekly). The diets and liraglutide treatment were maintained for 24 weeks before sacrifice. To monitor metabolic changes, body weight and fasting blood glucose were measured every four weeks during this period. As shown in Fig. 5B, most mice displayed a gradual weight increase. However, HFD-fed db/db mice reached peak body weight at week 12, followed by a decline, potentially indicating the onset of T2D symptoms. Consistent with liraglutide's known pharmacological effect on weight, the treatment group's body weight began to decline around week 16. Fasting blood glucose measurements (Fig. 5C) revealed hyperglycemia in all db/db mice, with the most pronounced increase observed in the HFD-fed db/db group. Conversely, liraglutide effectively controlled blood glucose levels in these mice. After 24 weeks, the animals were sacrificed, and myocardial tissue was collected for analysis. Picrosirius red staining of myocardial tissue sections (Fig. 5D) indicated more pronounced fibrosis in HFD-fed mice compared to the normal chow group, with the right atrium showing the highest fibrosis levels in HFD-fed db/db mice. Liraglutide treatment markedly reduced fibrosis, consistent with our in vitro findings in H9c2 cells. We further examined insulin resistance and lipid accumulation in myocardial tissue. Immunofluorescence staining results (Fig. 5E) showed significantly increased lipid accumulation in HFD-fed mice, particularly in db/db mice. These hearts also exhibited elevated pSer^{307}-IRS-1 expression, indicating insulin resistance. Liraglutide effectively reduced both lipid accumulation and insulin resistance in the myocardial

tissue of HFD-fed db/db mice, highlighting its potential in mitigating myocardial fibrosis.

Discussion

DbCM, a chronic disease characterized by complex interactions of metabolic and molecular mechanisms, is significantly impacted by prolonged glucolipotoxicity, resulting from the excessive accumulation of lipids within cardiomyocytes, particularly intracellular LDs [34]. This lipid overload is a critical factor in the development of cardiomyopathy and subsequent fibrosis, hallmark features of heart failure with preserved ejection fraction (HFpEF) [35]. HFpEF, a subtype of DbCM, is challenging to manage due to fibrosis-induced myocardial stiffness, which impairs diastolic function. Targeted interventions that modulate lipid metabolism could potentially prevent or slow fibrosis progression, thereby improving cardiac outcomes in diabetic patients [36]. Recent studies emphasize the therapeutic potential of pharmacological and lifestyle interventions, such as lipid-lowering drugs and dietary adjustments, to reduce myocardial lipid accumulation and fibrosis. For instance, Henry et al. highlighted the benefits of targeting lipid metabolic pathways on HFpEF [37], while others have demonstrated that preventing myocardial lipid accumulation may effectively inhibit DbCM progression [38]. Our findings support this approach, as GLP-1 RA liraglutide mitigated LD accumulation in myocardial cells caused by excessive glucose and free fatty acids (FFAs), thereby potentially alleviating cardiomyopathy by reducing fibrosis-related signaling and cellular oxidative stress.

Insulin resistance is also a significant contributor to myocardial pathology in diabetes, further exacerbated by glucolipotoxicity [39]. This dual metabolic burden increases oxidative stress, inflammation, and lipid accumulation, ultimately resulting in cardiac dysfunction and fibrosis [40]. GLP-1 RAs have emerged as promising therapeutic agents for DbCM due to their diverse cardioprotective effects [41]. Primarily, GLP-1 RAs enhance insulin signaling, essential for maintaining glucose homeostasis, and improve glycemic control, mitigating hyperglycemia-induced oxidative stress and inflammation associated with DbCM [42]. Improved insulin signaling reduces the metabolic burden on cardiac cells, preserving their function and preventing cardiomyopathy onset. Additionally, GLP-1 RAs activate the AMPK pathway, decreasing lipid accumulation and LD formation in cardiac cells [43]. AMPK, a crucial regulator of cellular energy homeostasis, promotes fatty acid catabolism, thereby reducing lipid load in cardiomyocytes. In our study, liraglutide, a GLP-1 RA, activated the AMPK pathway, enhancing fatty acid oxidation and decreasing lipogenesis, which reduced lipid-induced cardiomyopathy. Lower lipid accumulation is essential because lipotoxicity, linked to excessive LDs, induces cellular stress and promotes fibrosis development. By reducing lipid-induced stress and fibrosis, GLP-1 RAs help preserve myocardial structure and function [44]. The antifibrotic effects of GLP-1 RAs are partly mediated by AMPK activation, which inhibits fibrogenic signaling pathways [45]. Our findings also indicate that liraglutide downregulates TGF-β signaling, a key mediator of cardiac fibrosis, thus contributing to its cardioprotective effects by reducing fibrosis and enhancing myocardial function.

Our study further revealed that liraglutide enhances insulin signaling, restoring myocardial cells' ability to synthesize neurotrophic factors. DbCM frequently involves autonomic nervous system dysfunction, particularly sympathetic nerve atrophy in the right atrium [30]. Such nerve degeneration impairs cardiac output, reduces myocardial contractility, and diminishes heart rate variability, contributing to arrhythmias and heart failure. This nerve atrophy is exacerbated by glucolipotoxicity, which promotes oxidative stress, inflammation, and direct damage to myocardial cells [46]. The toxic accumulation of glucose and lipids in cardiac tissues also creates a hostile environment for peripheral nerve endings, increasing their susceptibility to degeneration. This loss of sympathetic innervation further compromises cardiac function, increasing the risk of arrhythmias and heart failure. Our findings demonstrate that liraglutide helps create a more supportive environment for peripheral nerve survival, consistent with the emerging understanding that cardiomyocytes, as secretory cells, play a role in maintaining and repairing surrounding tissue [47]. By preserving these secretory functions, liraglutide mitigates the adverse effects of glucolipotoxicity on cardiac cells. Despite these promising findings, further studies are warranted to confirm and expand upon these observations.

In conclusion, our research demonstrated that GLP-1 RA liraglutide confers protective effects in diabetic cardiomyopathy through multiple mechanisms, including AMPK pathway activation, which enhances insulin signaling efficiency, reduces lipid accumulation, and limits fibrosis. These mechanistic insights into GLP-1 RAs underscore their therapeutic potential for DbCM, offering a promising strategy to alleviate diabetes-related cardiac complications.

Author contributions Conceptualization, C.-Y. K., S.-H. T., C.-N. H., and C.-L. L.; methodology, S.-H. T., E. K. and C.-L. L.; validation, C.-L. L. and C.-N. H.; investigation, C.-Y. K., S.-H. T., E. K., K.-C. C. and K.-W. C.; resources, J.-C. L.; writing—original draft preparation, C.-Y. K., S.-H. T. and E. K.; writing—review and editing, C.-N. H. and

C.-L. L.; supervision, C.-N. H. and C.-L. L.; funding acquisition, E. K., S.-H. T., C.-L. L. and C.-N. H.

Funding This research was funded by the Chung Shan Medical University Hospital (CSH-2017-C-001 to E. K.), and the National Science and Technology Council of Taiwan (112-2320-B-040-003-MY3 to S.-H. T., 111-2314-B-040-029-MY3 to C.-N. H. and 111-2320-B-040-017-MY3 to C.-L. L.).

Data availability The data sets used and or analyzed during the current study are available from the leading corresponding authors on reasonable request.

Declarations

Conflict of interest The authors declare that they have no competing interests.

Ethical approval and consent to participate This research was established following the guidelines of the Institutional Animal Care and Use Committee (IACUC) of Chung Shan Medical University granted approval for this study with approval No. 2673.

Consent for publication All authors reviewed the results and approved this manuscript for publication.

References

1. Abudureyimu M, Luo X, Wang X, Sowers JR, Wang W, Ge J, Ren J, Zhang Y (2022) Heart failure with preserved ejection fraction (HFpEF) in type 2 diabetes mellitus: from pathophysiology to therapeutics. J Mol Cell Biol. https://doi.org/10.1093/jmcb/mjac028
2. Swiatkiewicz I, Patel NT, Villarreal-Gonzalez M, Taub PR (2024) Prevalence of diabetic cardiomyopathy in patients with type 2 diabetes in a large academic medical center. BMC Med 22:195. https://doi.org/10.1186/s12916-024-03401-3
3. Gulsin GS, Athithan L, McCann GP (2019) Diabetic cardiomyopathy: prevalence, determinants and potential treatments. Ther Adv Endocrinol Metab. https://doi.org/10.1177/2042018819834869
4. Huo JL, Feng Q, Pan S, Fu WJ, Liu Z, Liu Z (2023) Diabetic cardiomyopathy: early diagnostic biomarkers, pathogenetic mechanisms, and therapeutic interventions. Cell Death Discov 9:256. https://doi.org/10.1038/s41420-023-01553-4
5. Yu Y, Jin C, Zhao C, Zhu S, Meng S, Ma H, Wang J, Xiang M (2021) Serum free fatty acids independently predict adverse outcomes in acute heart failure patients. Front Cardiovasc Med 8:761537. https://doi.org/10.3389/fcvm.2021.761537
6. Tangvarasittichai S (2015) Oxidative stress, insulin resistance, dyslipidemia and type 2 diabetes mellitus. World J Diabetes 6:456–480. https://doi.org/10.4239/wjd.v6.i3.456
7. Tang Z, Wang P, Dong C, Zhang J, Wang X, Pei H (2022) Oxidative stress signaling mediated pathogenesis of diabetic cardiomyopathy. Oxid Med Cell Longev. https://doi.org/10.1155/2022/5913374
8. Zhou Y, Suo W, Zhang X, Liang J, Zhao W, Wang Y, Li H, Ni Q (2023) Targeting mitochondrial quality control for diabetic cardiomyopathy: Therapeutic potential of hypoglycemic drugs. Biomed Pharmacother 168:115669. https://doi.org/10.1016/j.biopha.2023.115669
9. Avagimyan A, Popov S, Shalnova S (2022) The pathophysiological basis of diabetic cardiomyopathy development. Curr Probl Cardiol 47:101156. https://doi.org/10.1016/j.cpcardiol.2022.101156
10. Huang W, Gao F, Zhang Y, Chen T, Xu C (2022) Lipid droplet-associated proteins in cardiomyopathy. Ann Nutr Metab 78:1–13. https://doi.org/10.1159/000520122
11. Cinato M, Andersson L, Miljanovic A, Laudette M, Kunduzova O, Borén J, Levin MC (2024) Role of perilipins in oxidative stress—Implications for cardiovascular disease. Antioxidants 13:209. https://doi.org/10.3390/antiox13020209
12. Muñoz-Córdova F, Hernández-Fuentes C, Lopez-Crisosto C, Troncoso MF, Calle X, Guerrero-Moncayo A, Gabrielli L, Chiong M, Castro PF, Lavandero S (2021) Novel insights into the pathogenesis of diabetic cardiomyopathy and pharmacological strategies. Front Cardiovasc Med 8:707336. https://doi.org/10.3389/fcvm.2021.707336
13. Saadat S, Noureddini M, Mahjoubin-Tehran M, Nazemi S, Shojaie L, Aschner M, Maleki B, Abbasi-Kolli M, Rajabi Moghadam H, Alani B, Mirzaei H (2020) Pivotal role of TGF-β/Smad signaling in cardiac fibrosis: non-coding RNAs as effectual players. Front Cardiovasc Med 7:588347. https://doi.org/10.3389/fcvm.2020.588347
14. Nikolov A, Popovski N (2022) Extracellular matrix in heart disease: focus on circulating collagen type I and III derived peptides as biomarkers of myocardial fibrosis and their potential in the prognosis of heart failure: a concise review. Metabolites 12:297. https://doi.org/10.3390/metabo12040297
15. Peng M-L, Fu Y, Wu C-W, Zhang Y, Ren H, Zhou S-S (2022) Signaling pathways related to oxidative stress in diabetic cardiomyopathy. Front Endocrinol (Lausanne) 13:907757. https://doi.org/10.3389/fendo.2022.907757
16. Graczyk P, Dach A, Dyrka K, Pawlik A (2024) Pathophysiology and advances in the therapy of cardiomyopathy in patients with diabetes mellitus. Int J Mol Sci 25:5027. https://doi.org/10.3390/ijms25095027
17. Arad M, Waldman M, Abraham NG, Hochhauser E (2020) Therapeutic approaches to diabetic cardiomyopathy: targeting the antioxidant pathway. Prostaglandins Other Lipid Mediat 150:106454. https://doi.org/10.1016/j.prostaglandins.2020.106454
18. Lam CSP, Chandramouli C, Ahooja V, Verma S (2019) SGLT-2 inhibitors in heart failure: current management unmet needs, and therapeutic prospects. J Am Heart Assoc 8:e013389. https://doi.org/10.1161/jaha.119.013389
19. Chen B, Guo J, Ye H, Wang X, Feng Y (2024) Role and molecular mechanisms of SGLT2 inhibitors in pathological cardiac remodeling (Review). Mol Med Rep 29:73. https://doi.org/10.3892/mmr.2024.13197
20. Joshi SS, Singh T, Newby DE, Singh J (2021) Sodium-glucose co-transporter 2 inhibitor therapy: mechanisms of action in heart failure. Heart 107:1032–1038. https://doi.org/10.1136/heartjnl-2020-318060

21. Schönberger E, Mihaljević V, Steiner K, Šarić S, Kurevija T, Majnarić LT, Bilić Ćurčić I, Canecki-Varžić S (2023) Immunomodulatory effects of SGLT2 inhibitors—Targeting inflammation and oxidative stress in aging. Int J Environ Res Public Health 20:6671. https://doi.org/10.3390/ijerph20176671
22. Gallo G, Volpe M (2024) Potential mechanisms of the protective effects of the cardiometabolic drugs type-2 sodium-glucose transporter inhibitors and glucagon-like peptide-1 receptor agonists in heart failure. Int J Mol Sci 25:2484. https://doi.org/10.3390/ijms25052484
23. Drucker DJ (2016) The cardiovascular biology of glucagon-like peptide-1. Cell Metab 24:15–30. https://doi.org/10.1016/j.cmet.2016.06.009
24. Zhang L, Tian J, Diao S, Zhang G, Xiao M, Chang D (2020) GLP-1 receptor agonist liraglutide protects cardiomyocytes from IL-1β-induced metabolic disturbance and mitochondrial dysfunction. Chem Biol Interact 332:109252. https://doi.org/10.1016/j.cbi.2020.109252
25. Ravic M, Srejovic I, Novakovic J, Andjic M, Sretenovic J, Muric M, Nikolic M, Bolevich S, Alekseevich Kasabov K, Petrovich Fisenko V, Stojanovic A, Jakovljevic V (2024) Effect of GLP-1 receptor agonist on ischemia reperfusion injury in rats with metabolic syndrome. Pharmaceuticals (Basel) 17:525. https://doi.org/10.3390/ph17040525
26. Almutairi M, Gopal K, Greenwell AA, Young A, Gill R, Aburasayn H, Al Batran R, Chahade JJ, Gandhi M, Eaton F, Mailloux RJ, Ussher JR (2021) The GLP-1 receptor agonist liraglutide increases myocardial glucose oxidation rates via indirect mechanisms and mitigates experimental diabetic cardiomyopathy. Can J Cardiol. 37:140–150. https://doi.org/10.1016/j.cjca.2020.02.098
27. Baggio LL, Yusta B, Mulvihill EE, Cao X, Streutker CJ, Butany J, Cappola TP, Margulies KB, Drucker DJ (2018) GLP-1 receptor expression within the human heart. Endocrinology 159:1570–1584. https://doi.org/10.1210/en.2018-00004
28. Bin Dayel F, Alonazi AS, Alrasheed NM, Alamin MA, Sarawi WS, Alharbi AO, Alabbad NA, Albuaijan DA, Alassiri DN, Aljarbua AF, Almusaytir FK, Alrasheed NM (2024) Role of the integrin-linked kinase/TGF-β/SMAD pathway in sitagliptin-mediated cardioprotective effects in a rat model of diabetic cardiomyopathy. J Pharm Pharmacol 76:64–73. https://doi.org/10.1093/jpp/rgad111
29. Prandi FR, Evangelista I, Sergi D, Palazzuoli A, Romeo F (2023) Mechanisms of cardiac dysfunction in diabetic cardiomyopathy: molecular abnormalities and phenotypical variants. Heart Failure Rev 28:597–606. https://doi.org/10.1007/s10741-021-10200-y
30. Sudo SZ, Montagnoli TL, Rocha BS, Santos AD, de Sá MPL, Zapata-Sudo G (2022) Diabetes-induced cardiac autonomic neuropathy: impact on heart function and prognosis. Biomedicines 10:3258. https://doi.org/10.3390/biomedicines10123258
31. Nguyen HC, Qadura M, Singh KK (2020) Role of the fatty acid binding proteins in cardiovascular diseases: a systematic review. J Clin Med 9:3390. https://doi.org/10.3390/jcm9113390
32. Zhou J, Poudel A, Chandramani-Shivalingappa P, Xu B, Welchko R, Li L (2019) Liraglutide induces beige fat development and promotes mitochondrial function in diet induced obesity mice partially through AMPK-SIRT-1-PGC1-α cell signaling pathway. Endocrine 64:271–283. https://doi.org/10.1007/s12020-018-1826-7
33. Peng D, Fu M, Wang M, Wei Y, Wei X (2022) Targeting TGF-β signal transduction for fibrosis and cancer therapy. Mol Cancer 21:104. https://doi.org/10.1186/s12943-022-01569-x
34. Cui X, Wang J, Zhang Y, Wei J, Wang Y (2022) Plin5, a new target in diabetic cardiomyopathy. Oxidat Med Cell Longev 2022:2122856. https://doi.org/10.1155/2022/2122856
35. Gollmer J, Zirlik A, Bugger H (2019) Established and emerging mechanisms of diabetic cardiomyopathy. J Lipid Atheroscler 8:26–47. https://doi.org/10.12997/jla.2019.8.1.26
36. Lin LC, Liu ZY, Yang JJ, Zhao JY, Tao H (2024) Lipid metabolism reprogramming in cardiac fibrosis. Trends Endocrinol Metabol TEM 35:164–175. https://doi.org/10.1016/j.tem.2023.10.004
37. Henry JA, Couch LS, Rider OJ (2024) Myocardial metabolism in heart failure with preserved ejection fraction. J Clin Med 13:1195. https://doi.org/10.3390/jcm13051195
38. Wang H, Wang J, Cui H, Fan C, Xue Y, Liu H, Li H, Li J, Li H, Sun Y, Wang W, Song J, Jiang C, Xu M (2024) Inhibition of fatty acid uptake by TGR5 prevents diabetic cardiomyopathy. Nat Metab 6:1161–1177. https://doi.org/10.1038/s42255-024-01036-5
39. Ma X, Liu Z, Ilyas I, Little PJ, Kamato D, Sahebka A, Chen Z, Luo S, Zheng X, Weng J, Xu S (2021) GLP-1 receptor agonists (GLP-1RAs): cardiovascular actions and therapeutic potential. Int J Biol Sci 17:2050–2068. https://doi.org/10.7150/ijbs.59965
40. Nakamura M, Sadoshima J (2020) Cardiomyopathy in obesity, insulin resistance and diabetes. J Physiol 598:2977–2993. https://doi.org/10.1113/jp276747
41. Jalil JE, Gabrielli L, Ocaranza MP, MacNab P, Fernández R, Grassi B, Jofré P, Verdejo H, Acevedo M, Cordova S, Sanhueza L, Greig D (2024) New mechanisms to prevent heart failure with preserved ejection fraction using glucagon-like peptide-1 receptor agonism (GLP-1 RA) in metabolic syndrome and in type 2 diabetes: a review. Int J Mol Sci 25:4407. https://doi.org/10.3390/ijms25084407
42. Wang Y, Cai F, Li G, Tao Y (2022) Novel dual glucagon-like peptide-1/ glucose-dependent insulinotropic polypeptide receptor agonist attenuates diabetes and myocardial injury through inhibiting hyperglycemia, inflammation and oxidative stress in rodent animals. Bioengineered 13:9184–9196. https://doi.org/10.1080/21655979.2022.2051859
43. Bu T, Sun Z, Pan Y, Deng X, Yuan G (2024) Glucagon-like peptide-1: new regulator in lipid metabolism. Diabetes Metab J 48:354–372. https://doi.org/10.4093/dmj.2023.0277
44. Withaar C, Meems LMG, Markousis-Mavrogenis G, Boogerd CJ, Silljé HHW, Schouten EM, Dokter MM, Voors AA, Westenbrink BD, Lam CSP, de Boer RA (2021) The effects of liraglutide and dapagliflozin on cardiac function and structure in a multi-hit mouse model of heart failure with preserved ejection fraction. Cardiovasc Res 117:2108–2124. https://doi.org/10.1093/cvr/cvaa256
45. Vandemark C, Nguyen J, Zhao ZQ (2023) cardiovascular protection with a long-acting GLP-1 receptor agonist liraglutide: an experimental update. Molecules (Basel, Switzerland) 28:1369. https://doi.org/10.3390/molecules28031369
46. Elshareif N, Gornick E, Gavini CK, Aubert G, Mansuy-Aubert V (2023) Comparison of western diet-induced obesity and streptozotocin mouse models: insights into energy balance, somatosensory dysfunction, and cardiac autonomic neuropathy. Front Physiol 14:1238120. https://doi.org/10.3389/fphys.2023.1238120
47. Berezin E, Berezin AA, Lichtenauer M (2021) Myokines and heart failure: challenging role in adverse cardiac remodeling, myopathy, and clinical outcomes. Dis Markers 2021:6644631. https://doi.org/10.1155/2021/6644631

Authors and Affiliations

Chien-Yin Kuo[1,2] · Sing-Hua Tsou[3] · Edy Kornelius[4,5] · Kuei-Chuan Chan[4,5] · Kai-Wei Chang[4] · Jung-Chi Li[6] · Chien-Ning Huang[1,4] · Chih-Li Lin[1,3]

✉ Chien-Ning Huang
cshy049@gmail.com

✉ Chih-Li Lin
dll@csmu.edu.tw

[1] Institute of Medicine, Chung Shan Medical University, No. 110, Sec. 1, Jianguo N. Rd, Taichung City 402, Taiwan

[2] Department of Surgery, Chung Shan Medical University Hospital, Taichung 402, Taiwan

[3] Department of Medical Research, Chung Shan Medical University Hospital, Taichung 402, Taiwan

[4] Department of Internal Medicine, Chung Shan Medical University Hospital, Taichung 402, Taiwan

[5] School of Medicine, Chung Shan Medical University, Taichung 402, Taiwan

[6] Department of Cardiology, Wuri Lin Shin Hospital, Taichung 414, Taiwan